Technical Paper
BR-1897

Comparison of Coal-Ash Corrosion Resistance of Alloys Exposed to Advanced Air-Coal and Oxy-Coal Combustion Environments

Authors:
S.C. Kung

Babcock & Wilcox
Power Generation Group, Inc.
Barberton, Ohio, U.S.A.

Presented to:
The Seventh International Conference on Advances in Materials Technology for Fossil Power Plants

Date:
October 22-25, 2013

Location:
Waikoloa, Hawaii, U.S.A.

B&W babcock & wilcox power generation group

Comparison of Coal-Ash Corrosion Resistance of Alloys Exposed to Advanced Air-Coal and Oxy-Coal Combustion Environments

Steven C. Kung, Ph.D.

Babcock & Wilcox Power Generation Group, Inc., Barberton, Ohio, U.S.A.

BR-1897
Presented to:
The Seventh International Conference on Advances in Materials Technology for Fossil Power Plants
October 22-25, 2013
Waikoloa, Hawaii, U.S.A.

ABSTRACT

A comprehensive research project consisting of pilot-scale combustion testing and long-term laboratory corrosion studies has been performed. A pilot-scale combustion facility was modified to enable burning pulverized coal under air-firing and oxy-firing conditions. Four United States (U.S.) coals were investigated, with the test conditions controlled so that both air-firing and oxy-firing tests of these coals had the same total heat input to the combustor. In addition, a calculated concentration of excess oxygen at 3% was implemented at the furnace outlet (equivalent to the furnace exit of a commercial utility boiler). For oxy-combustion, part of the flue gas was returned to the burner to simulate warm recycling in oxy-combustion, whereas for air firing, no gas recycling was involved. During each pilot-scale combustion test, online measurements of the flue gas were performed at the furnace outlet. In addition, deposit samples for chemical analysis were collected near the same location. The online gas measurements and deposit analyses allowed the combustion environments adjacent to the superheaters and reheaters of coal-fired boilers to be characterized under both air and oxy-firing conditions. The gas and deposit compositions were then simulated in a series of 1000-hour laboratory corrosion tests in which the corrosion performance of different alloys and weld overlays was evaluated at 1300^{o}F (704^{o}C).

Results of the laboratory study indicated that corrosion rates of the alloys and weld overlays exposed to the oxy-firing conditions were no worse than those of the corresponding air-firing conditions, even though the sulfur dioxide (SO_2) and hydrogen chloride (HCl) concentrations in the combustion gas of oxy-firing were three to four times of those of air-firing. It is proposed that the better corrosion performance of these materials was attributed primarily to high carbon dioxide (CO_2) concentrations present in the oxy-combustion gas, which increased the density of the gas phase. As a result, diffusion of the corrosive species in the porous deposit was retarded. In addition, the initial amount of sulfate-based salt in the oxy-firing deposit was lower than that in the corresponding air-firing deposit due to the presence of carbonate. The conversion of carbonate to sulfate is highly favored thermodynamically but would take some time to complete. A reduction in the availability of fused sulfate led to less hot corrosion attack, at least during the early stage of the laboratory exposures. Furthermore, CO_2 and HCl gases are highly acidic in nature and would reduce the basicity of the sulfate melt once the initially protective oxide scale formed was penetrated. With a lower basicity, the basic solubility of metal oxides in fused sulfate and the slope of a negative solubility gradient were decreased, thereby reducing the severity of hot corrosion attack via the classic dissolution and fluxing mechanism. The formation of carbonate and chloride solutes in fused sulfate would only take place when the partial

pressures of oxygen (O_2) and sulfur trioxide (SO_3) was extremely low, a condition anticipated at the scale/metal interface after scale penetration.

INTRODUCTION

The recent development of high-efficiency, low-emission coal-fired utility boilers has led to steam conditions of much higher temperatures and pressures.[1] Examples include the development of advanced ultra supercritical (A-USC) boiler systems that may push the steam temperatures up to 760°C (1400°F) and pressures up to 35 MPa (5000 psi). While a higher efficiency and lower emission can be realized from these advanced combustion systems, the steam conditions inevitably demand the use of increased creep-resistant alloys for the construction of superheaters and reheaters. Under these steam conditions, accelerated fireside corrosion is a particular concern for the high-temperature sections of boiler tubes in the upper furnace. The higher steam temperatures will raise the metal temperatures of superheaters and reheaters significantly, leading to an increased propensity for coal ash corrosion (also known as hot corrosion).[2,3] The highest coal ash corrosion attack would likely occur in the superheater and reheater outlet banks, with the tube OD temperatures ranging from 650 to 815°C (1200 to 1500°F) and corrosion rates peaking near 1300°F (704°C).

Results of numerous materials studies have been reported in the literature, mainly comparing the corrosion resistance of alloys and coatings exposed to the fireside environments of coal-fired utility boilers.[3-5] However, the results of most of these studies were produced from laboratory studies under relatively simplified test conditions. Since knowledge of the actual combustion environments existing in coal-fired boilers is generally lacking, especially for those species most critical to fireside corrosion, the majority of the laboratory studies have implemented conditions that were derived from either thermodynamic calculations of the combustion systems or measurements of product gases from slow pyrolysis of small coal samples in a batch process.[7-11] Test conditions determined from neither approach can fully represent the dynamic nature of coal combustion in commercial coal-fired utility boilers.

In recent years, the implementation of oxy-coal combustion has been considered as a viable means to capture CO_2 produced from coal-fired power plants. Oxy-combustion involves partial recycling of the combustion gas back to the boilers through the primary and secondary gas streams in a closed boiler system. Besides the primary purpose of increasing gas velocity, gas recycling can also enrich CO_2 to a concentration level that is economical for downstream capturing, compression, and purification. As the combustion gas recycles, the concentrations of corrosive species in the gas phase, such as SO_2 and HCl, are also increased if they are not completely scrubbed prior to the return of the combustion gas. This is especially true for the case of “hot” and “warm” recycling designs in which the concentrations of the corrosive species can be three to four times of those in corresponding air-fired boilers burning the same coal. Such an increase in concentration could pose significant concerns for the long-term reliability and performance of oxy-fired boilers.

Various corrosion data from extensive research studies pertaining to oxy-combustion are available in the literature. However, these data are often inconsistent and at times controversial. A careful review of these studies revealed that the majority have employed test conditions that did not properly reflect those anticipated for oxy-combustion in coal-fired commercial boilers. In fact, some of the laboratory tests were performed under environments that deviated so greatly from those anticipated for oxy-coal combustion that they should not even be considered relevant. Therefore, a comprehensive and systematic study is needed to quantify the impact of oxy-combustion on the fireside corrosion of superheaters and reheaters in coal-fired A-USC boilers.

Towards this goal, a study consisting of a series of pilot-scale combustion tests and laboratory corrosion exposures has been performed. During the pilot-scale testing phase, the concentrations of various gaseous species generated from the air and oxy-combustion of each of four U.S. coals were measured online, while deposit samples were collected for analyses. For oxy-combustion, part of the flue gas was returned to the burner via warm recycling. The gas measurements and deposit analyses allowed the combustion environments near the superheaters and reheaters of coal-fired A-USC boilers to be realistically characterized under both firing modes. The gas and deposit compositions were then carefully simulated in a series of 1000-hour laboratory corrosion tests in which the corrosion resistance of different alloys and weld overlays was evaluated at 704°C (1300°F). The corrosion rates of the materials evaluated under both air and oxy-firing conditions of the four coals are compared here, and the corrosion mechanisms operating in coal-fired A-USC boilers are proposed.

EXPERIMENTAL PROCEDURES

Four U.S. coals, different greatly in composition and property, were selected for this corrosion study. The proximate and ultimate analyses, chlorine contents, and heating values of these coals are compared in Table 1. Per ASTM International classifications,[12] Wyoming (WY) Powder River Basin (PRB) is ranked as sub-bituminous, while the other three coals are bituminous. The sulfur contents of these coals ranged from high (4.31%) in *OH Gatling* to low (0.25%) in *WY PRB*. The chlorine contents also varied significantly from nearly 0.4% in *IL #6 Galatia* to below 10 ppm in *WY PRB*. The moisture content was relatively high in the PRB coal compared to those of the bituminous. All of these coals were processed and pulverized to a particle size of 70% passing 200-mesh, the same fineness requirements for commercial coal-fired utility boilers.

Table 1
As-Received Ultimate Analysis, Proximate Analysis, Chlorine Content, and Higher Heating Value for Four U.S. Coals Investigated

As Received wt.%	IL #6 Galatia	WY PRB	OH Mahoning 7A	OH Gatling
Proximate Analysis				
Moisture	5.40	24.59	2.22	3.77
Ash	8.65	5.14	9.92	11.34
Vol. Matter	35.68	37.00	40.79	40.73
Fixed Carbon	50.27	33.27	47.07	44.16
Total	100.00	100.00	100.00	100.00
Ultimate Analysis				
Moisture (%)	5.40	24.59	2.22	3.77
Hydrogen (%)	3.74	2.55	4.18	4.07
Carbon (%)	70.16	54.75	74.67	67.11
Nitrogen (%)	1.04	0.83	0.93	0.94
Sulfur (%)	2.69	0.25	1.96	4.31
Oxygen (%)	8.32	11.89	6.12	8.46
Ash (%)	8.65	5.14	9.92	11.34
Total (%)	100.00	100.00	100.00	100.00
Chloride (%) (wet basis)	0.3693	0.0010	0.1946	0.0373
Heating Value				
Heating Value (Btu/lb)	12,575	9,156	13,404	12,191
Ash Analysis				
Silicon Dioxide, % as SiO2	48.12	36.04	42.65	40.35
Aluminum Oxide, % as Al2O3	19.65	16.84	29.07	22.56

Iron Oxide, % as Fe2O3	17.64	5.86	20.45	28.33
Calcium Oxide, % as CaO	4.28	21.61	1.76	2.62
Magnesium Oxide, % as MgO	0.95	5.06	0.52	0.69
Sodium Oxide, % as Na2O	1.08	1.69	0.34	0.41
Potassium Oxide, % as K2O	2.59	0.50	1.61	1.28
Titanium Dioxide, % as TiO2	1.05	1.32	1.41	1.04
Manganese Dioxide, % as MnO2	0.07	0.02	0.00	0.05
Phosphorus Pentoxide, % as P2O5	0.08	1.00	0.76	0.22
Strontium Oxide, % as SrO	0.03	0.35	0.12	0.09
Barium Oxide, % as BaO	0.05	0.62	0.07	0.11
Sulfur Trioxide, % as SO3	4.41	9.09	1.24	2.25
Alkalies as Na20	2.79	2.02	1.40	1.25
Base to Acid Ratio	0.39	0.64	0.34	0.52
Silica Ratio	0.68	0.53	0.65	0.56
T250, °F	2429	2228	2497	2295

Combustion tests of the four coals were performed in a pilot-scale testing facility rated nominally at 160 kW by thermal input. The test facility, shown in Figure 1, was capable of producing a down-fired, swirl-stabilized coal flame in a cylindrical combustion chamber of 265 cm in height and 75 cm in inner diameter. The inner surface of the combustion chamber was water-cooled and lined with a high-temperature refractory. The inset in Figure 1 depicts the coal burner of the pilot-scale testing facility, with streamlines showing the mixture of primary gas and fuel flowing through the center feed tube and secondary gas swirling around the primary mix. A swirling secondary gas stream is an important feature of modern burners to achieve superior air/fuel mixing, stabilized flame, and reduced NO_x formation.[13] The combustion chamber of the pilot-scale test facility consisted of a series of view ports that offered easy access for probe insertions and thus online gas measurements and deposit collections at the locations of interest. For oxy-combustion, a signification modification was made to the pilot-scale test facility by converting the gas flow from once-through to oxy-firing with warm gas recycling.

For pilot-scale combustion testing, the coal and gas flow rates were adjusted for both air and oxy-firing conditions of each coal so that (1) an approximately 160 kW thermal input was achieved in the pilot-scale test facility, and (2) 3% theoretical excess oxygen required for coal combustion was maintained at the furnace outlet. An online gas sampling system was used to measure the concentrations of gaseous species present in the oxidizing zone of the pilot-scale test facility.[14]

Table 2 summarizes the gas compositions determined from the pilot-scale combustion study of the four U.S. coals under both air and oxy-firing conditions. As mentioned previously, the flue gas was once-through in the air-firing combustion tests but warm-recycled in oxy-firing. Only the major and selected gases are listed here, as the presence of other species, including various hydrocarbon and some sulfur and chlorine-bearing compounds, were insignificant. Elemental sulfur (S_2) and chlorine (Cl_2) and were not included in the online measurements due to their thermodynamic instability in combustion gas at the combustion temperatures. Based on detailed analysis of the gaseous species produced from the air combustion of eight U.S. coals, Kung[14] concluded that the SO_2 and HCl concentrations present in the gas phase of oxidizing zone at the furnace exit essentially accounted for all the S and Cl in coal.

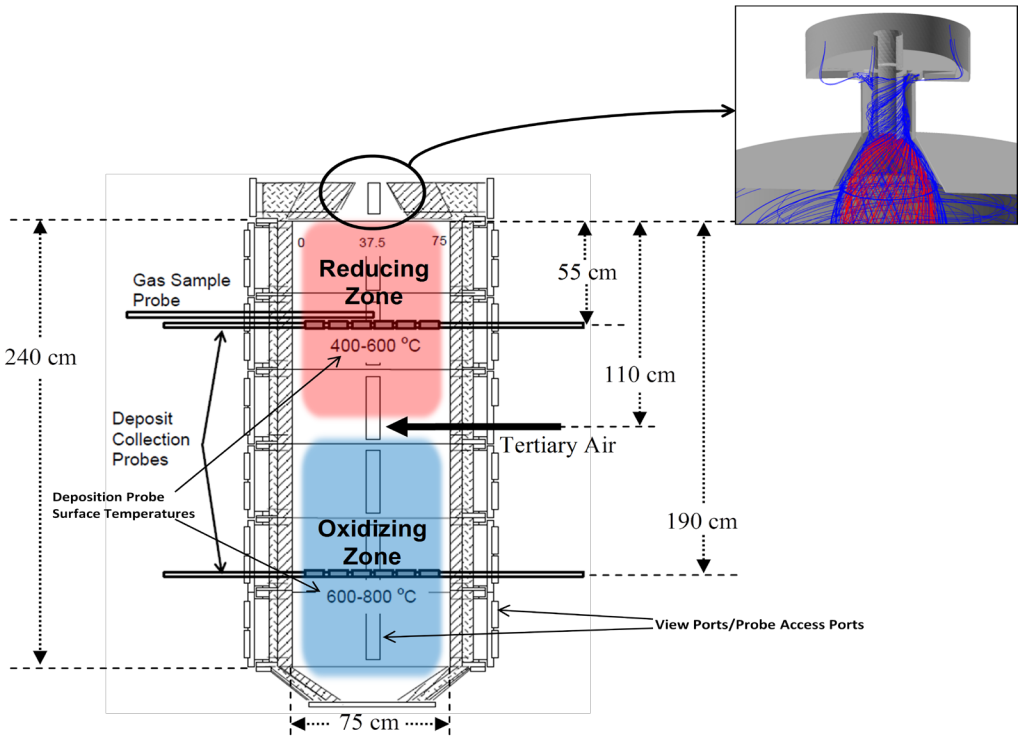

Figure 1 - Schematic Diagram of the Pilot-Scale Combustion Facility.

Table 2
Representative Gas Compositions Measured in the Oxidizing Zone of Pilot-Scale Testing Facility during Combustion of Four Selected Coals under Air and Oxy-combustion Conditions

	IL #6 Galatia		OH Mahoning 7A		OH Gatling		WY Black Thunder PRB	
	Air	Oxy	Air	Oxy	Air	Oxy	Air	Oxy
O_2	3.00%	2.90%	3.00%	3.00%	3.00%	3.00%	3.00%	3.00%
CO_2	16.00%	74.17%	16.00%	75.61%	15.00%	71.32%	17.00%	67.17%
CO		0.0340%		0.0162%		0.0078%		0.0167%
H_2O	7.00%	17.80%	9.00%	19.16%	7.00%	18.49%	12.00%	26.71%
SO_2	0.2300%	0.6240%	0.1550%	0.3880%	0.2700%	1.0340%	0.0200%	0.0640%
H_2S		0.0267%						
HCl	0.0200%	0.0640%	0.0110%	0.0346%	0.0005%	0.0055%		0.0001%
N_2	73.75%	4.40%	71.83%	1.79%	74.73%	6.14%	68.00%	3.04%

As expected, Table 2 reveals a major shift in concentration between air and oxy firing from the enrichment of nitrogen gas (N_2) for the former to CO_2 for the latter. In addition, a significant increase in the moisture content was observed for the oxy firing conditions. Important to fireside corrosion, the SO_2 and HCl concentrations measured from oxy-combustion with warm recycle were three to four times of those of corresponding air-firing cases. In addition, the SO_2 and HCl concentrations increased proportionally with increasing S and Cl contents in the coal, with the highest HCl concentration observed for the *IL #6 Galatia* coal and highest SO_2 for *OH Gatling*. Note that the SO_2 concentration for the oxy-combustion of *OH Gatling* exceeded 1% in the gas phase. Obviously, such a high concentration of corrosive species must be avoided in boiler design. However, for the objective of this study, it is

beneficial to quantify the extent of the impact on fireside corrosion from oxy-combustion of extremely high sulfur (and Cl) coals.

Table 2 also reveals the presence of some carbon monoxide (CO) (78-340 ppmv) at the furnace exit for the oxy-combustion of all four coals, even though the overall gas compositions at this location was highly oxidizing (contained ~3% O_2). Furthermore, some hydrogen sulfide (H_2S) was detected with a FTIR at this oxidizing location during the oxy-combustion of *IL #6 Galatia*. The detection of these reducing species clearly indicates that the kinetics of oxy-coal combustion are more sluggish than those of air combustion, as no measurable amounts of CO and H_2S were observed for all of the air-firing cases. Therefore, even though the combustion gases were not fully equilibrated in the oxidizing zone of air-firing, as concluded by Kung,[14] a further deviation from equilibrium was evident for oxy-coal combustion. Slower reaction kinetics are expected for oxy-combustion due to a reduced flame temperature compared to that of corresponding air-firing based on the same amounts of oxygen and coal burned. A lower flame temperature would inevitably delay char burnout in the burner zone and result in less completion of the coal combustion at the furnace exit. It should be pointed out that the concentrations of CO_2 and H_2S were relatively small so that the combustion gas should not be considered reducing.

Table 3 summarizes the deposit compositions implemented for the laboratory study. Obviously, the compounds of sulfate, carbonate, and chloride would contribute more importantly to fireside corrosion than those of oxide, and these compounds were all readily available commercially. Due to the instability of potassium oxide (K_2O) at room temperature, the compound of KOH was used when needed, which would quickly decompose upon heating to form the desired K_2O.

Table 3
Compositions of Coal Ash Deposit Used in the Laboratory Fireside Corrosion Tests Under Air and Oxy-Firing Conditions

	IL #6 Galatia		OH Mahoning 7A		OH Gatling		WY Black Thunder PRB	
	Air	Oxy	Air	Oxy	Air	Oxy	Air	Oxy
Al_2O_3	11.11	11.35	16.92	16.68	13.36	13.78	17.89	10.97
SiO_2	24.42	26.83	22.62	23.00	21.27	21.52	31.80	28.78
CaO	2.18	3.17	0.89	0.71	0.97		21.24	8.91
Fe_2O_3	10.37	7.59	7.78	8.13	13.50	14.25	5.09	0.45
K_2TiO_3					0.90			0.60
KOH	0.68	0.72	1.02	1.02			0.83	
TiO_2	0.41	0.44	0.62	0.62		0.45	1.20	0.30
$MgSiO_3$	0.95		0.30				4.19	
$Fe_2(SO_4)_3$	17.31	22.70	19.84	14.59	17.77	18.95		26.75
$KAl(SO_4)_2$		0.30		0.25	0.40			
$CaSO_4$		0.05			0.05			0.30
$K2SO_4$	4.84	6.68	4.84	3.74	16.77			
$MgSO_4$	10.03		10.07				12.27	12.70
$Na2SO_4$	17.71	0.95	15.11	1.84	1.90		5.49	7.15
$CaCO_3$		8.13		4.13	2.60	16.55		
$K2CO_3$		0.80		0.60	0.90	6.45		
$MgCO_3$		6.53		15.59	6.31	4.60		3.10
Na_2CO_3		3.64		9.11	3.30	3.45		
NaCl		0.01						
KCl		0.04						
$FeCl_3$		0.07						

Several high-temperature alloys and two weld overlays were evaluated in the laboratory study for the potential application of superheaters and reheaters in coal-fired A-USC boilers, as shown in Table

4. Duplicate samples of each material were prepared and included in each of the laboratory tests, with one for dimensional measurements and the other for metallographic examinations. The initial dimension of each test sample was approximately 1¼" x ¾" x thickness, where the thicknesses of the monolithic alloys and weld overlays were approximately 1/8" and 0.070", respectively. Samples of the weld overlays were EDM-removed from weld-overlaid boiler tubes after the OD surface was machined. Consequently, both curved surfaces of each weld-overlay sample were smooth for thickness measurements.

After sample preparation, the test specimens were placed in high-purity alumina crucibles and filled with the deposit mixtures shown in Table 3. These crucibles were then transferred to a horizontal retort inside a high-temperature furnace with both ends properly sealed. A schematic of the laboratory retort/furnace system employed is presented in Figure 2. At the end of each 1000-hour test, corrosion rates of the alloys and weld overlays were calculated based on the measured weight and thickness losses.

Table 4
Compositions of Alloys and Weld Overlays Evaluated in Laboratory Study

	T23	304H	S304H	310HCbN	230	347HFG	347H	72WO	52WO	740	617	120	800H
Ni		11	8.73	19.97	59.5	11.98	10.42	47.2	56.3	49.45	53.2	37.3	32.7
Cr	2.18	18.83	18.68	25.61	21.31	18.4	17.67	>41.2	29.6	24.31	22.63	25.1	21.0
Fe		Bal	67.6	Bal	1.25	Bal	68.4	10.6	12.2	1.02	0.76	34.7	Bal.
Mo	0.21		0.32	-	1.28	-	0.24	0.07	0.03	0.52	9.38	0.27	-
Co			0.14	-	0.14	-	< 0.1	0.02	0.003	19.63	12.33	0.10	-
C	0.084	0.05	0.084	0.05	0.088	0.09	0.045	0.023	0.029	0.034	0.06	0.06	0.08
N	0.0076		0.11	0.24		-	-			-	-	0.20	-
B	0.001		-	-	0.005	-	-	-	-	-	0.002	-	-
Mn	0.50	1.8	0.8	1.18	0.51	1.46	1.84	0.11	0.29	-	0.02	0.71	0.80
Si	0.25	0.45	0.14	0.36	0.45	0.41	0.44	0.16	0.2	0.45	0.15	0.48	0.59
Al	0.027	-	-	-	0.44	-	-	0.14	0.7	0.75	1.15	0.059	0.45
Ti		-	-	-	-	-	-	0.44	0.53	1.58	0.27	-	0.31
Nb	0.034	-	0.52	0.47	0.053	-	-			1.83	-	0.61	-
Nb+Ta		-	-	-	-	0.9	-	0.02	0.02	-	-	-	-
V	0.25	-	<0.1	-	0.011	-	-	0.02	0.02	-	-	-	-
W	1.46	-		-	14.93	-	-	ND	ND	-	-	0.10	-
Cu		-	2.78	-	-	-	0.35	0.03	0.02		0.05	-	0.11
P	0.009	0.01	-	0.015	-	0.027	0.026	-	-	-	-	-	-
S	<0.001	0.013	-	-	-	0.001	0.003	-	-	-	0.001	-	<0.002
Other		-	-	-	-	-	-	-	0.058	-	-	-	-

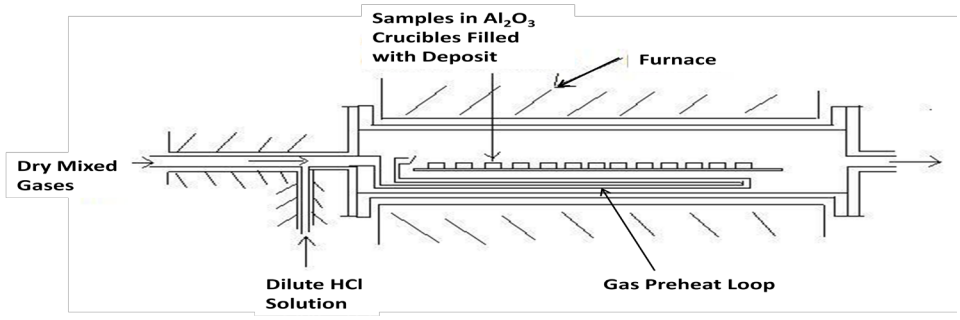

Figure 2 - Schematic of Retort/Furnace System Employed for the Laboratory Fireside Corrosion Study

RESULTS AND DISCUSSION

Figure 3 summarizes the corrosion rates of the alloys and weld overlays exposed to various laboratory test conditions at 704°C (1300°F), which simulated the air and oxy-combustion of four U.S.

coals in Table 1. The corrosion rates are expressed in mils per year (mpy) that were calculated and extrapolated linearly from the 1000-hour test data. For each coal, the corrosion rates of alloys and weld overlays from the oxy-firing conditions are compared directly to those of air-firing. For ease of comparison, the scale on Y-axis is fixed for all plots. For the X-axis, the materials are arranged in the order of increasing Cr concentration from left to right, which included ferritic steel (T23), austenitic stainless steels (347H, 347HFG, Super 304H, 304H, 800H, and 310HCbN), nickel-base alloys (230, 617, 740H, and 120), and weld overlays (52WO and 72WO). Note that the T23 sample was not available for testing in the air-firing exposures of *IL #6 Galatia* and *WY PRB* coals. Therefore, only the corrosion rates determined from the oxy-firing conditions are included in Figure 3.

Many interesting findings are immediately apparent from the results of the laboratory study in Figure 3. First, almost all of the materials evaluated in this study exhibit a lower corrosion rate for oxy-firing than that of air-firing. This comparison is especially amazing when considering the concentrations of the corrosive species (in particular SO_2 and HCl gases) employed in the oxy-combustion tests were three to four times of those in the corresponding air-firing cases. Only a very few of these data pairs displayed a reversed trend, and essentially all of the reversal was associated with relatively low corrosion rates measured. It is likely that, when the corrosion rates were low, a higher degree of experimental uncertainty was involved in the measurements, thus making the absolute rate comparison less reliable. For those alloys suffering high corrosion attack, the air-firing environments were consistently more corrosive than the oxy-firing conditions.

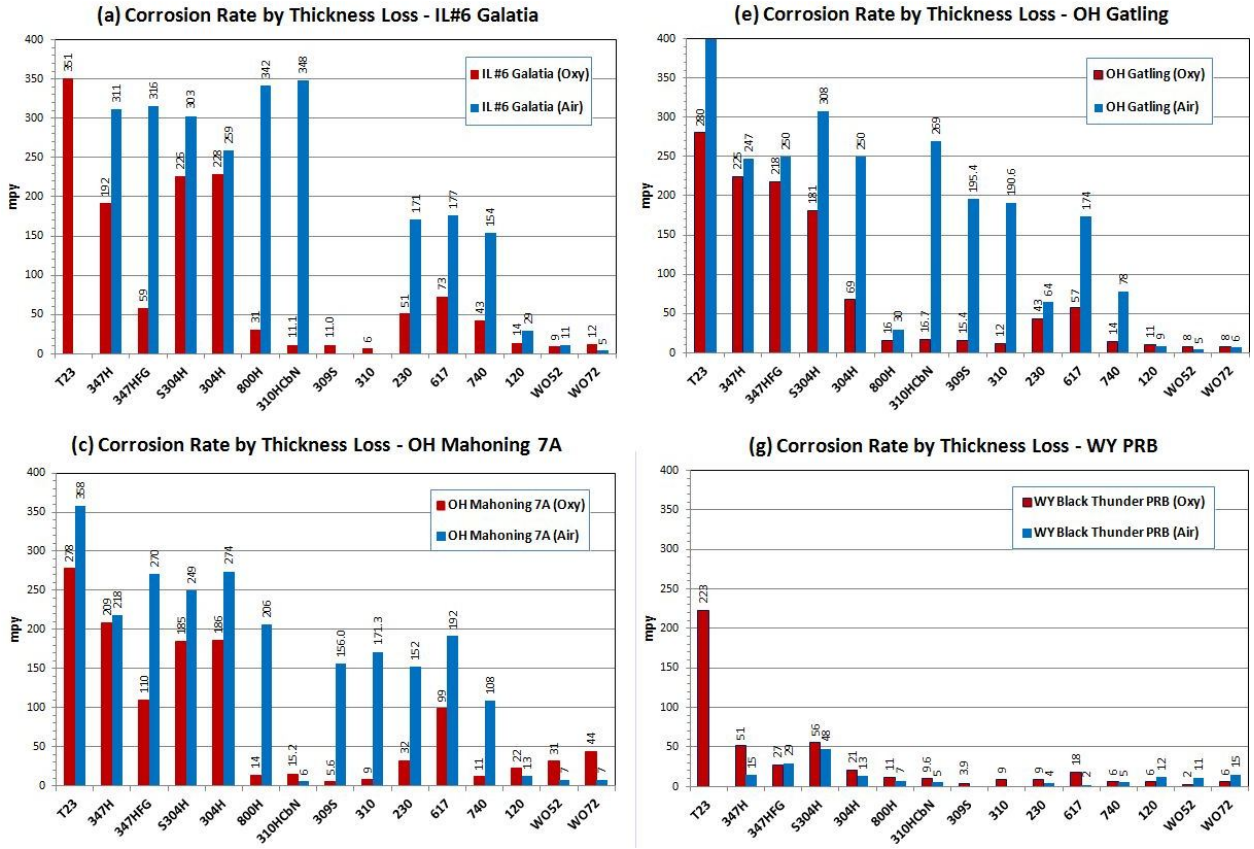

Figure 3 - Comparison of Linear Corrosion Rates in mpy for Alloys and Weld Overlays Exposed to Laboratory Corrosion Tests at 704°C (1300°F) for 1000 Hours under Air-Firing and Oxy-Firing Conditions.

In general, the materials exposed to the combustion environments of *IL #6 Galatia* coal produced the highest corrosion rates among the four coals studied, followed by *OH Gatling* and *OH Mahoning*. There are only a few exceptions to this trend, which would have been attributed to specific reactions between the combustion environments and elements in the alloys. The corrosion rates of the higher alloys and weld overlays measured from the *WY PRB* tests were quite low compared to those of the other three coals. Obviously, these low rates reflected the very low sulfur and essentially zero chlorine contents in this coal. Even when the amounts of SO_2 and HCl were increased three to four times in the gas phase by switching the combustion mode from air-firing to oxy-firing (with warm recycling) for this coal, the resulting concentrations of these species were still too low to cause severe fireside corrosion.

One exception to the generally low corrosion rates found in the PRB test conditions is the T23 ferritic steel. With the absence of air-firing kinetics data, the corrosion rates of T23 from oxy-combustion exhibited slightly lower but comparable values to those of the other coals containing much higher sulfur and chlorine contents. In fact, all of the corrosion rates for T23 appeared to stay within a narrow range among the four coals, despite that the corrosion rates for T23 should have been noticeably higher than those of the highly corrosion-resistant alloys investigated. From this research work, it was uncovered that, due to the lack of sufficient Cr content in the low-Cr ferritic steel, the alloy did not have the ability to form a more protective oxide scale on the surface upon exposure to the highly oxidizing/sulfidizing combustion gases in the upper furnace of advanced coal-fired boilers. As a result, a scale morphology consisting of both iron oxide and iron sulfide was produced on the metal surface underneath the porous deposit. With the iron sulfide exposed to the HCl-containing gases in the deposit, a new mechanism of "active sulfidation-oxidation" was identified, which will be discussed shortly.

Extensive SEM/EDS examinations were performed on the polished cross-sections of the exposed samples. All cross-sections were cut and polished with kerosene to preserve any water-soluble compounds present in the deposit. A backscattered SEM micrograph and the associated EDS elemental maps for the corrosion product and surface deposit of 309S exposed to the air-firing *OH Gatling* test are shown in Figure 4. The *OH Gatling* coal contained high sulfur (4.31%) and extremely high contents of sulfates of iron (Fe), potassium (K), and magnesium (Mg) in the deposit. Accordingly, the mixed gas employed in the laboratory condition for this coal contained the highest SO_2 partial pressure in the gas phase among all the air-firing tests. The micrograph and elemental maps show two clearly different types of corrosion behavior, spanning from portion of a pit to un-pitted surface.

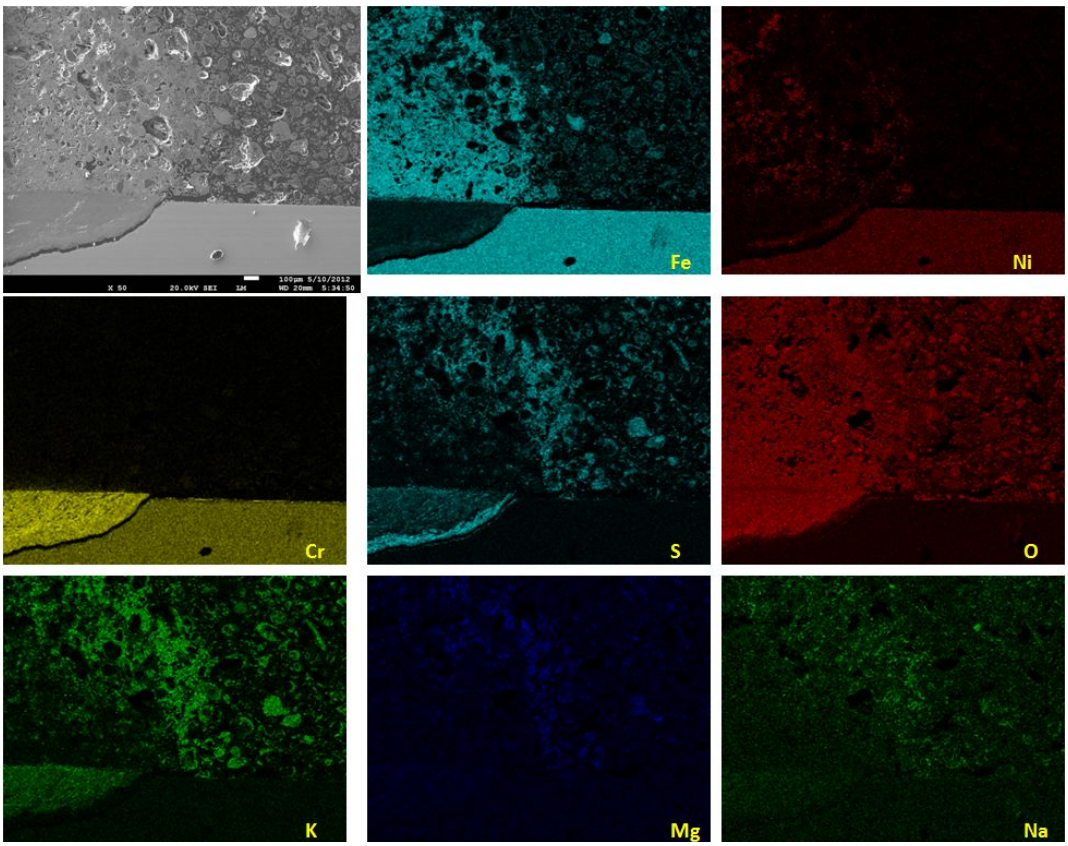

Figure 4 - Backscattered SEM Micrograph of Corrosion Scale and Portion of Deposit Layer on 309S after Exposure to Air-Firing OH Gatling Oxidizing Conditions for 1000 Hours at 704°C (1300°F).

Over some part of the alloy, a thin protective scale rich in Cr_2O_3 was present (as shown on right-hand side of the micrograph), but otherwise there were pits penetrating into the alloy. The deposit structure and composition over the pits are significantly different from those of the protected area. Sulfur is found concentrated at the base of the pits, along with nickel and the alkali elements. From the elemental maps of Figure 4, chromium (Cr) is concentrated in the pit but not outside (above) the pit in the deposit. To the contrary, Fe and nickel (Ni) are essentially absent in the pit, and Ni has clearly migrated into a dense, hemispherical phase in the deposit above the pit. Even though the ash deposit already contained Fe, the detection of a greater amount of iron in the deposit above the pit clearly suggests that additional Fe has migrated from the pit into the deposit above. No chlorine was found anywhere on this cross-section.

These characteristics are consistent with the classic hot corrosion mechanism that involves basic fluxing of solutes from the oxides of Ni and Fe, followed by re-precipitation of these oxides out in the deposit where their solubility are lower. The fluxing and re-precipitation are dictated by a negative solubility gradient for these “basic” oxides, as proposed by Rapp and Goto.[15] A high local salt basicity in the pit has been generated by local penetration of the protective scale, formation of sulfide, and the release of oxide ions into the sulfate melt. Likewise, because the obvious occurrence of the fused salt in the corrosion deposit was localized, it is assumed that a liquid phase was stabilized by the lowering of the liquidus via an interaction of the salt with a corrosion product, perhaps nickel sulfide. The Cr oxide

solute must have experienced a positive solubility gradient in the pit, as no evidence for its outward migration in Figure 4. In fact, the concentration of Cr exhibits a step change from the pit to the Fe_2O_3 and NiO re-precipitated zone above, a morphology characteristic of the basic dissolution and fluxing mechanism.

Figure 5 shows a backscattered SEM micrograph and the associated elemental maps for the cross-section of 309S after exposure to the oxy-firing *OH Gatling* laboratory condition at 704°C (1300°F) for 1000 hours. The surface morphology of 309S from the oxy-firing test can be compared directly to those of air-firing in Figure 4. It should be emphasized that magnification of the images in Figure 5 is five times of that in Figure 4. Therefore, the worst localized attack and penetration found on 309S from the oxy-firing test in Figure 5 is much shallower than those of air-firing in Figure 4. Such a low corrosion attack observed for 309S under the oxy-firing condition is clearly consistent with the significant difference in the measured corrosion rates reported in Figure 3, in spite of the SO_2 and HCl concentrations employed in the oxy-firing test being three to four times of those in the air-firing case. Reasons for the reduced corrosion rates in oxy-firing environments will be discussed later.

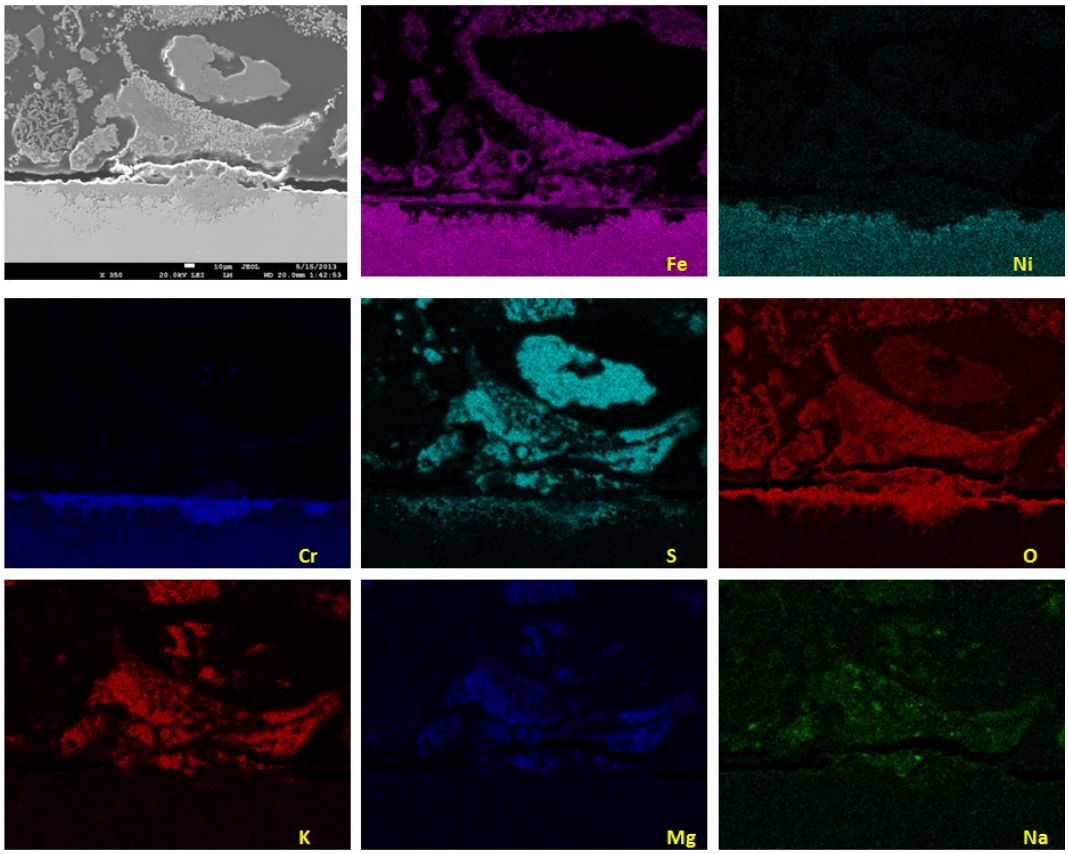

Figure 5 - Backscattered SEM Micrograph of Corrosion Scale and Portion of Deposit Layer on 309S after Exposure to Oxy-Firing OH Gatling Oxidizing Conditions for 1000 Hours at 704°C (1300°F).

Except for the obvious difference in corrosion rate, the morphology of the corrosion product formed on 309S from oxy-firing is identical to that of air-firing. As mentioned above, these features consist of outward flux and re-precipitation of the solutes of Fe and Ni oxides in the pit by fused sulfate

after the initially protective scale was locally penetrated. Chromium remained in the scale, with no detectable amount found in the re-precipitation zone above the pit. Like the air-firing case, no evidence of corrosion attack from chlorine was observed on the cross-section of 309S (or any other samples from this test) under the oxy-firing condition. Therefore, the corrosion mechanism operating on the superheaters and reheaters of oxy-fired A-USC boilers burning the *OH Gatling* coal is expected to be dictated by the hot corrosion mechanism involving fused sulfate.

Similar SEM/EDS results were observed for all of the austenitic stainless steels and nickel-base alloys. A generalization for these higher alloys can be made here, in which a sulfur-rich scale was generally present under the scale in contact with the alloy, and a continuous fused sulfate salt existed throughout the corrosion product. Chromium was enriched in the salt phase beneath the deposit where both iron and nickel were depleted but found deposited in the adjacent deposit layer. Upon scale penetration, chemical reactions between the fused sulfate and metals led to the formation of metal sulfide and the release of oxide ions that significantly increased the salt basicity locally at the metal/scale interface. Consequently, the basic solutes of NiO and Fe_3O_4, i.e., M_2NiO_2 and $MFeO_2$, respectively, were formed and diffused out in the salt down a negative solubility gradient. These solutes re-precipitated out as non-protective oxide particles of Ni and Fe in the salt phase within the deposit. The basic solute for chromium oxide (probably Na_2CrO_4), in contrast, did not diffuse out because of a positive solubility gradient for the chromate ion resulting from a strong oxygen-pressure dependence for its solubility.[15] No corrosion attack associated with chlorine was observed, including *IL #6 Galatia* under the oxy-firing condition where an extremely high concentration of HCl was measured in the pilot-scale combustion facility and subsequently employed in the laboratory test.

An entirely different corrosion morphology was observed for the low-Cr ferritic steel of T23. Figure 6 shows an optical micrograph of the corrosion scale and deposit layer exfoliated from a T23 sample exposed to the air-firing combustion environment of *OH Gatling* coal with high S but negligible Cl at 704°C (1300°F). The heterogeneous multi-layered scale and deposit shown in Figure 6 exhibited little variation in layer thicknesses along the height of the test sample immersed vertically in the crucible filled with the simulated deposit. Thus, oxidant diffusion through the porous deposit did not contribute significantly to the rate controlling step or product chemistry, which is consistent with the expectation for high-temperature corrosion involving a porous medium.

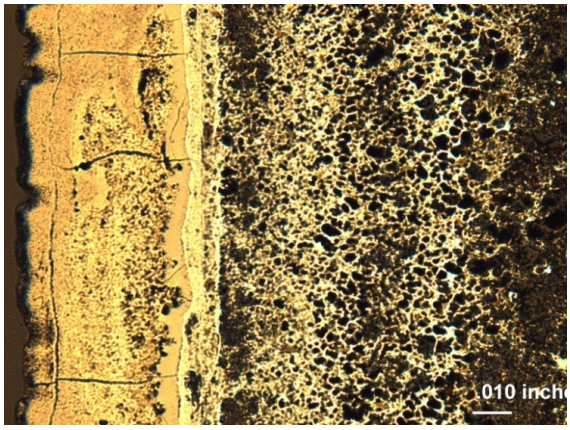

Figure 6 - Optical Micrograph of Corrosion Scale and Portion of Deposit Layer Spalled off from T23 after Exposure to Air-Firing OH Gatling Oxidizing Conditions for 1000 Hours at 704°C (1300°F).

The scale morphology of T23 exhibited a rather layered and patchy structure. The dense phase in contact with the alloy substrate (now separated from the scale) at the left-hand side of the micrograph is about 8-mil thick and is predominantly Fe-Cr oxide (probably Fe-Cr spinel). This spinel layer was likely the innermost oxide scale formed initially and was somewhat protective. Farther out into the scale (toward the right), a similar dense phase consists again of Fe-Cr oxide (still spinel) with a thickness of approximately 35-40 microns. Patchy porous areas are embedded in this outer spinel scale, which contain both iron oxide and iron sulfide. The outermost portion of the compact scale is also mostly Fe-Cr oxide and is probably magnitite. Further out to the bright yellow layer as well as the stringers intermixed with the particles of the deposit, the presence of potassium is evident. Figure 7 shows the backscattered SEM micrograph and associated elemental maps for the middle section of the scale/deposit layer in Figure 6. The elemental maps for Fe and Cr indicate a sharp boundary between the compact corrosion scale and the deposit layer, which is also consistent with the maps for the deposit elements of K, silicon (Si) and aluminum (Al) (Si and Al maps are not shown) that are all confined to the deposit layer but not in the compact scale. These characteristics do not resemble those consistent with the hot corrosion attack discussed previously for the austenitic stainless steels and nickel-base alloys.

Generally, farther out in the deposit, above the compact (dark orange) corrosion scale in Figure 6, both potassium and magnesium were found associated with sulfur, likely to be mixed sulfates. Most importantly, in this porous zone of ash deposit, a lacey iron oxide arising from substrate oxidation was present at a distance several times the thickness of the compact scale layer. A zone relatively depleted in sulfur is seen between the top of the compact corrosion scale and sulfate particles farther out in the deposit. The observation of iron oxide far out into and intermixed with the porous ash deposit can only be understood in terms of an “active volatile-chloride-supported oxidation” process of iron sulfide at the base of the deposit in contact with the gas phase that contained HCl molecules. Such a corrosion process for low-alloy ferritic steel is named here as the Active Sulfidation-Oxidation Mechanism. The proposed active sulfidation-oxidation mechanism differs in detail from the active oxidation mechanism proposed by Grabke, et al.[16,17] for corrosion of alloys by a much more oxidizing gas in the presence of municipal waste deposits. In that case, the active oxidation mechanism was proposed to occur by the formation of volatile $FeCl_2$ (and even condensed $FeCl_2$) from iron oxide at the base of the deposit and the conversion of volatile $FeCl_2$ to iron oxide farther out in the deposit with the release and recycling of molecular chlorine (Cl_2).

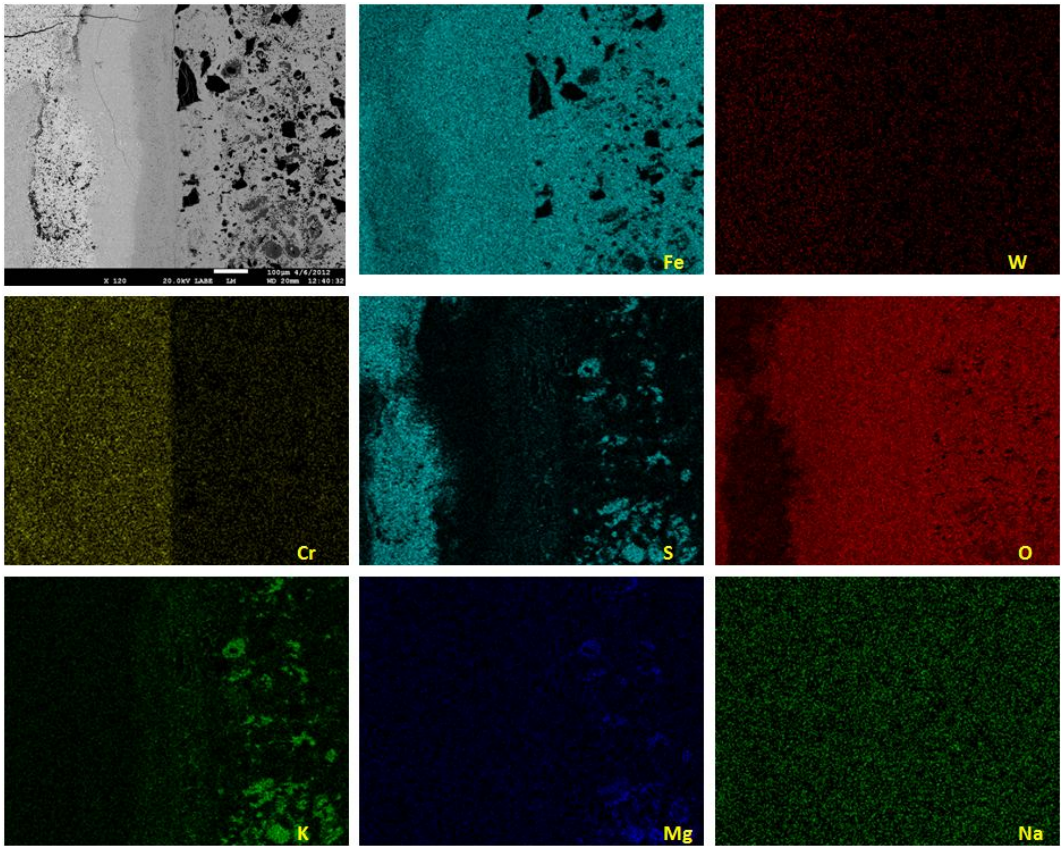

Figure 7 - SEM Micrograph and Associated Elemental Maps of Corrosion Scale and Portion of Deposit Layer Spalled off from T23 after Exposure to Air-Firing OH Gatling Oxidizing Conditions for 1000 Hours at 704°C (1300°F).

In the less oxidizing but more sulfidizing environment of the current study, iron sulfide is seen to exist to the extremity of the compact scale, and this FeS would have a much higher thermodynamic activity for iron than the neighboring iron oxide phase. Therefore, the volatile $FeCl_2$ would form from iron sulfide instead of iron oxide, but would be deposited as a particulate oxide farther out in the deposit. This mechanism can be expressed by the following reaction.

$$FeS + 2\ HCl\ (g) + 2\ O_2\ (g) = FeCl_2\ (g) + H_2O\ (g) + SO_3\ (g) \qquad \text{Eq. 1}$$

where the Gibbs energy of reaction for Eq. 1 is approximately -112 kcal/mole.

While converting condensed FeS to $FeCl_2$ vapor, Eq. 1 also served as a catalyst to convert SO_2 to SO_3. Such a chemical reaction was proven experimentally in this study by analyzing the SO_3 concentrations exiting the testing retort. Results of the in-situ gas analyses during the corrosion exposures showed that about 25% of the SO_2 entering the retort was converted to SO_3. After its formation, the SO_3 would either diffuse outward from the base of the porous deposit to the bulk gas or react with oxides of alkalis, rare earth metals, and iron oxide to form more sulfate in the deposit.

After the $FeCl_2$ vapor is transported away from the base of the deposit via gas phase diffusion, subsequent oxidation of this vapor would occur via Eq. 2, resulting in the condensation of iron oxide far out in the deposit where the gas composition is sufficiently oxidizing, i.e.,

$$FeCl_2\ (g) + H_2O\ (g) + 1/4\ O_2\ (g) = \tfrac{1}{2}\ Fe_2O_3 + 2\ HCl\ (g) \qquad \text{Eq. 2}$$

where the Gibbs energy of reaction for Eq. 2 is approximately -42 kcal/mole.

The conversion of $FeCl_2$ vapor to condensed Fe_2O_3, followed by the return of HCl product gas to the base of the deposit, could sustain the looping reactions of Eqs. 1 and 2. Incidentally, the *OH Gatling* coal was not (at all) one of the high-Cl coals studied. Therefore, higher corrosion rates would be expected for low-alloy steels exposed to the combustion environments of coals of higher chlorine contents, as evidenced in Figure 3.

For comparison, an optical micrograph of the scale/deposit layer exfoliated from the T23 sample exposed to the oxy-firing *OH Gatling* coal condition is shown in Figure 8. The morphology of this scale/deposit combination from the oxy-firing test resembles closely to that of Figure 6 from the corresponding air-firing test, except that the thicknesses of the scale and iron oxide condensed in the porous deposit are less. Such a close resemblance clearly suggests that the corrosion mechanism operating on T23 was identical under both air-firing and oxy-firing conditions. However, the corrosion rate from oxy-firing was lower than that of air-firing, consistent with the corrosion rates shown in Figure 3. Similar morphologies were also found on T23 for the test conditions of other coals, except that of air-firing PRB where no chlorine was introduced. These results indicate that the "active sulfidation oxidation mechanism" would likely operate on low-Cr ferritic steels even at a very low concentration level of HCl in the gas phase.

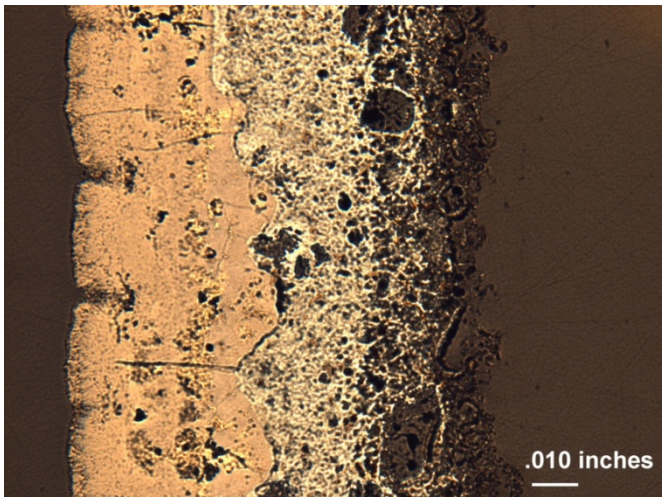

Figure 8 - Optical Micrograph of Corrosion Scale and Portion of Deposit Layer Spalled off from T23 after Exposure to Oxy-Firing OH Gatling Oxidizing Conditions for 1000 Hours at 704°C (1300°F).

It should be emphasized that only for the low-alloy steel is FeS seen as a secondary corrosion product contacting the gas phase at the base of the deposit. For the higher alloys investigated, even if metal sulfides were formed at the base of the corrosion scale, they were not in direct contact with the HCl-bearing combustion gas due to their ability to form a more protective scale. Since the vapor pressure of $FeCl_2$ is proportional to the thermodynamic activity of Fe as well as the partial pressure of HCl (squared), the vapor pressure of $FeCl_2$ would be too low to support the active sulfidation-oxidation

mechanism. Consequently, none of the higher alloys produced the lacey iron oxide condensate in the ash deposit, indicating no FeS phase had reached the surface of the scale at the base of the deposit.

The better corrosion performance of the alloys and weld overlays under the oxy-combustion conditions than the air-firing cases could be explained by three key reasons. First, the diffusivity of corrosive species in the oxy-firing combustion gas is lower than that in air-firing. Wall et al.[18] pointed out that, because the molecular weight of CO_2 is 44 and N_2 is 28, a higher density was expected for the oxy-firing combustion gas. By a first order of approximation, the density of oxy-firing combustion gas is about 1.6 times that of the corresponding air-firing case, i.e., 44÷28=1.6. Because of the higher density, the diffusivity of O_2 in CO_2 was reported by Wall et al. to be 0.8 time that in N_2. The authors did not compare the relative diffusivities of SO_2 and HCl in CO_2 and N_2 gases, respectively.

However, the difference in density alone could not account for all the differences in the measured corrosion rates between air and oxy-firing. The deposit chemistry must have also played a role. The deposit compositions for oxy-firing contained a significant amount of alkali and alkaline earth metal carbonate. The presence of carbonate in the deposit collected from the furnace outlet of the pilot-scale testing facility implied that the combustion kinetics were more sluggish for oxy-firing than air-firing, possibly due to a higher heat capacity of CO_2 than that of N_2 (and thus lower combustion temperatures for oxy-firing). It is also possible that the higher density of oxy-firing combustion gas discussed above reduced gas phase diffusivity of the combustion gas. Both a reduced gas temperature and diffusivity would have delayed coal combustion and char burnout in the burner zone. Under the air-firing conditions, only the *OH Gatling* coal exhibited some carbonate in the deposit, although its amount was smaller than that of the corresponding oxy-firing sample. It should be pointed out that carbonate in the deposit should not be considered as unburned carbon (UBC).

Thermodynamically, sulfate of alkali and alkaline earth metal is much more stable than carbonate. In fact, the difference in stability is so huge that the presence of any carbonate will be chemically converted to sulfate as long as a very small amount of sulfur exists in the system. It is unclear, however, how fast the conversion would take place kinetically. Obviously, the carbonate included in the laboratory deposit had fully converted to sulfate during the 1000-hour exposure of each test, since no evidence of any carbonate was found in the deposit from the SEM/EDS examinations. However, it is also conceivable that the conversion process took some time to complete. Because hot corrosion is fueled by the amount of sulfate available in the deposit, which has been demonstrated here as the predominant mechanism attacking the higher alloys and weld overlays under both air and oxy-firing conditions, the lower availability of sulfate in the oxy-firing cases would reduce the severity of the corrosion attack, at least initially, compared to the corresponding air-firing conditions until all carbonate was fully sulfated. Accordingly, the formation of carbonate from oxy-coal combustion in A-USC boilers could be considered a “beneficial” factor.

The third reason leading to the reduced corrosion attack in oxy-firing combustion environments would be the reduction of salt basicity from a much higher concentration of CO_2, and possibly HCl too, compared to those in the corresponding air-firing conditions. As mentioned previously, upon penetration of the initially protective scale, fused sulfate becomes extremely basic (and reducing) due to rapid reactions between the salt and metal. The higher the salt basicity, the higher the basic solubility is for the solutes of oxides of the alloying elements. In addition, the higher the salt basicity, the greater the negative solubility gradient is for the dissolved solutes. A high basic solubility and solubility gradient would have been responsible for the rapid hot corrosion attack observed for the austenitic stainless steels and nickel-base alloys exposed to the air-firing conditions. However, when the CO_2 and HCl

concentrations were increased in the gas phase from oxy-firing, the acidic nature of these gases would have partially neutralized the basicity of the fused salt via the following examples.

$$CO_2\ (g) + \underline{Na_2O} = \underline{Na_2CO_3} \qquad \text{Eq. 3}$$

$$2\ HCl\ (g) + \underline{Na_2O} = 2\ \underline{NaCl} + H_2O\ (g) \qquad \text{Eq. 4}$$

where the underlined species denote either a basic component of the fused salt or reaction products that become (dissolved) solutes in the fused salt. Similar reactions can be written for other basic components, such as K_2O, MgO, and CaO.

When these basic components of fused sulfate were neutralized by the acidic gases of CO_2 and HCl, both the basic solubility of metal oxides and their concentration gradients were decreased. As a result, the hot corrosion attack of higher alloys and weld overlays from fused sulfate in the oxy-firing combustion gas was noticeably reduced kinetically compared to that in air-firing. In comparison, the impact of the neutralization effect on salt chemistry would be greater for CO_2 than that HCl due to their significant difference in concentration. It is also possible that the formation of a higher concentration of acidic SO_3 in the gas phase per Eq. 1 has also helped neutralize the basicity of the fused salt in hot corrosion. Because the SO_3 concentrations would likely to be even lower than those of HCl, its benefit in the reduction of hot corrosion attack from oxy-firing was probably small.

It is likely that the impact from the first reason, i.e., decreased diffusivity from a higher gas density, has impacted more on the vapor transport of $FeCl_2$ in the corrosion of T23 via the newly proposed active sulfidation-oxidation mechanism. As mentioned earlier, the reduction in gas phase diffusivity from oxy-firing is not expected to be significant compared to that of air-firing. Therefore, the benefit arisen from reduced gas diffusivity in oxy-firing coal combustion would be relatively small. Such a smaller improvement is clearly demonstrated in Figure 3 where a slightly lower corrosion rate of T23 is seen for oxy-firing than that in the corresponding air-firing. For the attack dominated by the hot corrosion mechanism on higher alloys and weld overlays, the latter two reasons, i.e., delayed availability of the sulfate and especially the reduction of salt basicity from the acidic gases, would have played a more prominent role. These two reasons would impact the corrosion performance of alloys significantly by modification of the salt chemistry in the deposit. Consequently, a more dramatic improvement was generally observed on the measured corrosion rates in Figure 3 for the higher alloys and weld overlays when the combustion mode was switched from air-firing to oxy-firing.

CONCLUSIONS

A comprehensive research project consisting of pilot-scale combustion testing and long-term laboratory corrosion study has been performed. A pilot-scale testing facility was modified to enable the combustion of four pulverized U.S. coals under both air-firing and oxy-firing conditions. For each of these coals, the test conditions were controlled so that both air-firing and oxy-firing tests had the same total heat input to the combustor and the excess oxygen at the furnace exit was 3%. For oxy-combustion, part of the flue gas was returned to the burner to simulate warm recycling in oxy-combustion, whereas for air-firing, no gas recycling was involved. The partial flue gas recycling led to a CO_2 concentration in the combustion gas at approximately 70%.

During each pilot-scale combustion test, online measurements of the flue gas were performed at the furnace outlet with a FTIR and GC. In addition, deposit samples were collected near the same location. The online gas measurements and deposit analyses allowed the combustion environments

adjacent to the superheaters and reheaters of coal-fired boilers to be more realistically characterized under both air-firing and oxy-firing conditions. The gas and deposit compositions were then simulated in a series of 1000-hour laboratory corrosion tests in which the corrosion resistance of different alloys and weld overlays was evaluated at 704°C (1300°F).

Results of the laboratory study revealed that corrosion rates of the alloys and weld overlays exposed to the oxy-firing conditions were no worse than those of the corresponding air-firing conditions. In fact, lower corrosion rates were generally observed for the materials tested under the oxy-combustion environments at 704°C (1300°F) with few exceptions, even though the SO_2 and HCl concentrations in the gas phase of oxy-combustion cases were three to four times of those of air-firing.

Based on the extensive metallurgical examinations and SEM/EDS analyses performed, a pattern of behavior has been concluded for the higher alloys and weld overlays exposed to a wide range of coal environments at 704°C (1300°F). First, the classic hot corrosion mechanism dominated the corrosion process under both air-firing and oxy-firing conditions, with the possible exception of the very low sulfur *WY PRB* coal. The austenitic stainless steels and nickel-base alloys showed the initial formation of a Cr-rich protective scale that was eventually penetrated by fused sulfate to permit much more rapid attack via basic dissolution and fluxing of the initially protective oxide scales formed.

An entirely different corrosion mechanism was identified for the low-Cr ferritic steel of T23. Due to a relatively low Cr content in this alloy, the corrosion scale consisted of iron oxide and iron sulfide formed under the highly sulfidizing and oxidizing environments, with the sulfide phase in direct contact with the HCl-bearing combustion gas at the base of the porous deposit. As a result, the corrosion attack on T23 was governed by a looping reaction of "active sulfidation-oxidation mechanism," in which FeS reacted with HCl to form $FeCl_2$ vapor, followed by outward diffusion of $FeCl_2$ into the porous deposit and re-precipitation as iron oxide upon exposure to a higher partial pressure of oxygen. This proposed active sulfidation-oxidation mechanism was responsible for the unusually high wastage rates of T23 and would likely dominate the corrosion attack of other low-Cr steels also.

It is proposed that the superior corrosion performance of the materials studied under the oxy-firing conditions was attributed primarily to higher CO_2 concentrations in the combustion gas. First, the higher CO_2 concentrations increased the density of the combustion gas, leading to reduced diffusivity of corrosive gases, such as SO_2, HCl, and $FeCl_2$. The decrease in diffusivity would be primarily responsible for the improvement in the corrosion performance of T23 when the combustion mode was changed from air-firing to oxy-firing. Secondly, the initial amount of sulfate salt available in the oxy-firing deposit was lower than that in the corresponding air-firing deposit due to the significant formation of carbonate. The conversion of carbonate to sulfate would have taken some time to complete, thus reducing the availability of sulfate needed to initiate hot corrosion.

Most importantly, CO_2 and HCl gases are highly acidic in nature and would reduce the basicity of fused sulfate once the initially protective oxide scale was penetrated. The reduction in basicity could be achieved by CO_2 and HCl reacting with the basic components of the sulfate melt to form carbonate and chloride solutes, hence reducing the local basicity of the liquid. With a reduced basicity, the basic solubility of metal oxides and the slope of a negative solubility gradient were decreased, thereby reducing the severity of the hot corrosion attack via basic dissolution and fluxing. The formation of carbonate and chloride solutes in fused sulfate would take place only when the partial pressures of O_2 and SO_3 are low, a condition existing at the scale/metal interface. Because the concentrations of CO_2 in

the oxy-coal combustion gases are orders of magnitude higher than those of HCl, the reduction in salt basicity from the former is likely to be more significant than the latter.

ACKNOWLEDGEMENT

The author would like to acknowledge the funding support of two U.S. Department of Energy projects: DE-FC26-07NT43097 (PM: Vito Cedro) and DE-FG26-01NT41175 (PM: Patricia Rawls). Professor Robert A Rapp served as a technical consultant and contributed significantly to the success of this study.

REFERENCES

1. R. Viswanathan, R. Purgert, and U. Rao, "Materials Technology for Advanced Coal Power Plants," Journal of Materials Engineering and Performance, Vol. 14, No. 3, June 2005.
2. R. A. Rapp and Y. S. Zhang, "Hot Corrosion of Materials: Fundamental Studies," Journal of Metals, Vol. 46, No. 12, pp. 47-55, 1994.
3. S. C, Kung, "Fireside Corrosion in Coal- and Oil-Fired Boilers," ASM Handbook, 13C, 2006.
4. W.A. Bakker, "Materials for Advanced Boilers," Advanced Heat Resistant Steels for Power Generation, R. Viswanathan and J.W. Nutting, ed., IOM Communications Ltd., London, 1999, p. 435.
5. L. A. Ruth and N. Birks, "Materials Needs for High Efficiency Coal Fired Boiler Plants," Int'l Sym. On Ultra-High Temperature Materials, Tajimi, Japan, 1995.
6. J. Blough and W. T. Bakker, "Measurement of Superheater Corrosion Caused by Molten Alkali Sulfates," Heat Resistant Materials, Proc. 1st Int'l Conf., ASM International, 1991, p. 567.
7. P. L. Daniel, "The Effect of Coal Chlorides on Furnace Wall Corrosion," Coal Science and Technology 17 Chlorine in Coal, J. Stringer and D. D. Banerjee, Ed., Elsevier Science Publishing Co., 1991, p.207.
8. R. C. John, W. C. Fort III, and R. A. Tait, Mat'ls at High Temp., V. 11, No. 1-4, 1993, p. 124.
9. L. Duan, C. Zhao, W. Zhou, C. Qu, and X. Chen, "Investigation on Coal Pyrolysis in CO_2 Atmosphere." *Energy & Fuels*, 23(7), 3826-3830, 2009.
10. V. P. Kaminskii, "The Mechanism of How Several Components of the Flame Form and Act on the Tube Metal of the Waterwalls of Power Boilers when Burning Anthracite Culm." Thermal Engineering, 43(6), 505-510, 1996.
11. R.K. Srivastava, C.A. Miller, C. Erickson, and R. Jambhekar, "Emissions of Sulfur Trioxide from Coal-fired Power Plants." Journal of the Air & Waste Management Association, 54(6), 750-762, 2004.
12. ASTM Standards, "Standard Classification of Coals by Rank," D388-95, 1995.
13. Burners and Combustion Systems for Pulverized Coal, Chapter 12, Steam/Its Generation and Use, 41st ed., The Babcock & Wilcox Company, 2005.
14. S. C. Kung, "Measurement of Corrosive Gaseous Species in Staged Coal Combustion," Oxid. Met., 77, 289–304, 2012.
15. R.A. Rapp and K.S. Goto, "The Hot Corrosion of Metals by Molten Salts", Molten Salts II, R. Selman and J. Braunstein, Eds., Electrochem. Soc., Princeton (1979) p.159.
16. H.J. Grabke, E. Reese and M. Spiegel, Molten Salt Forum, Vol. 5-6, (1998), 405-11.
17. H. J. Grabke, "Kinetics of Interfacial Reactions of Gases on Metals and Oxides", Proceedings of International Conference on High Temperature Corrosion, NACE (1980), pp. 287-94.
18. T.F. Wall, et al.,, "An Overview on Oxyfuel Coal Combustion-State of the Art Research and Technology Development," Chem. Eng. Res. Design, 87, 1003-1016, 2009.

Disclaimer

Although the information presented in this work is believed to be reliable, this work is published with the understanding that the Babcock & Wilcox Power Generation Group, Inc. (B&W PGG) and the authors are supplying general information and are not attempting to render or provide engineering or professional services. **Neither B&W PGG nor any of its employees make any warranty, guarantee, or representation, whether expressed or implied, with respect to the accuracy, completeness or usefulness of any information, product, process, method, or apparatus discussed in this work, including warranties of merchantability and fitness for a particular or intended purpose. Neither B&W PGG nor any of its officers, directors, or employees shall be liable for any losses or damages with respect to or resulting from the use of, or the inability to use, any information, product, process, method, or apparatus discussed in this work.**